Robotica (2015) volume 33, pp. 986–1002. © Cambridge University Press 2014
doi:10.1017/S0263574714000733

Teleoperation grasp assistance using infra-red sensor array

Nutan Chen†§*, Keng Peng Tee‡ and Chee-Meng Chew†

†*Department of Mechanical Engineering, National University of Singapore, Singapore, 117576 SG*
‡*Institute for Infocomm Research, A*STAR, Singapore, 138632 SG*
§*Faculty for Informatics, Technical University Munich, Munich, Germany, 80333 DE*

(Accepted February 22, 2014. First published online: March 24, 2014)

SUMMARY
Teleoperated grasping requires the abilities to follow the intended trajectory from the user and autonomously search for a suitable pre-grasp pose relative to the object of interest. Challenges include dealing with uncertainty due to the noise of the teleoperator, human elements and calibration errors in the sensors. To address these challenges, an effective and robust algorithm is introduced to assist grasping during teleoperation. Although without premature object contact or regrasping strategies, the algorithm enables the robot to perform online adjustments to reach a pre-grasp pose before final grasping. We use three infrared (IR) sensors that are mounted on the robot hand, and design an algorithm that controls the robot hand to grasp objects using the information from the sensors' readings and the interface component. Finally, a series of experiments demonstrate that the system is robust when grasping a wide range of objects and tracking slow-moving mobile objects. Empirical data from a five-subject user study allows us to tune the relative contributions from the IR sensors and the interface component so as to achieve a balance of grasp assistance and teleoperation.

KEYWORDS: Shared control; Grasping; Teleoperation; Human–robot interaction; IR sensor.

1. Introduction

Grasping is one of the most fundamental actions required of a service robot. Robots that are able to grasp objects by teleoperation can assist humans in performing special or routine activities, such as essential tasks of drinking, and more complex actions of doing housework in a kitchen.

There are many examples of teleoperation for manipulation and grasping.[1–7] Humans can grasp objects easily because they are good at object localization and hand–eye coordination, and have the ability to learn a variety of methods for grasping different objects. However, a human perceives an object differently during teleoperation due to poor depth information. Also, uncertainty is introduced due to the difference in the dimensions of human and robot arms. A user requires training and experience in operating the robot to ensure effective use of the system. Even for skillful users, uncertainties from sensor noise and calibration errors are unavoidable factors that limit performance.

Based on the challenges of teleoperation mentioned above, it is necessary to improve grasping in real-time using sensors for adjusting the end-effector when the hand is close to an object. It is a sensitive task requiring object perception to determine/locate the grasp points for an object. Strategies employed in object perception are based on co-planarity and colour information captured by stereo cameras,[8] learning grasp strategies using partial information[9] and range scanning sensors based on 3D model reconstruction.[10]

Middle- or long-range sensors, such as laser scanner[11] and stereo cameras,[12] can detect and localize objects fairly accurately, but these are not suitable for teleoperation. Firstly, occlusion by the robot arm may occur during manipulation of the object. Secondly, image acquisition and processing are

* Corresponding author. E-mail: nutan@in.tum.de

https://doi.org/10.1017/S0263574714000733 Published online by Cambridge University Press

generally not fast enough for online reactive response in unstructured environments (e.g. when the object is moving).

Tactile sensors have been employed as well in refs. [13, 4], but they are contact-based sensing methods. For teleoperation, contacting objects are almost as difficult as grasping them.

Short-range stereo cameras[15] mounted on the end-effector have been developed. However, they have a narrow field of view and cannot be positioned at short distances from the object, otherwise there may not be any suitable grasp points. In addition, the data from the stereo cameras are large and have a high computation cost.

Pre-touch sensing, whose sensing range is between those of tactile sensors and vision, has been employed for short-range perception. Smith *et al.*[16] and Wistort and Smith[17] describe electric field (EF) pre-touch, which aligns robot arms with objects and pre-shapes the fingers for grasping. Unfortunately, EF pre-touch is highly sensitive to the objects' material. In another work,[18] two different designs are presented for different applications using seashell effect pre-touch. One of the strategies detects the surface for sensing extremely compliant objects, but only one side of the PR2 gripper is mounted with the sensor. Consequently, it cannot guarantee the object in the middle of the gripper and might cause an unsuccessful grasping. Object scanning is required for another strategy to add pre-touch pointcloud of the unknown portions of an object, which is difficult to apply for real-time grasping. Optical infrared (IR) sensors are also introduced for pre-touch during final grasp adjustments. Although these have less information compared with cameras or lasers, these are less sensitive to environmental changes and require less computation. The method in ref. [19] detects the orientation of an object surface using the IR sensors that fit inside the fingers. Continuous shared control[20] combines brain signal and IR sensors to grasp object. However, IR sensors in Hsiao *et al.*[19] can only adjust the fingers, and that in Kim *et al.*[20] can only be used for one dimension of the end-effector. In ref. [21], IR sensors are attached on a gripper to aid in positioning the gripper to apply a normal force to object boundary. However, the objects are supposed to be in the gripper before applying the method and it uses logic approach.

In the area of navigation, potential energy is widely used for obstacle avoidance[22] in two dimensions, but it is seldom used for grasping. Compared with navigation, our algorithm not only assists the robot hand to avoid collision but also enables the hand to move to a graspable position.

In this paper, an approach of grasp assistance for teleoperation using three IR sensors is presented. It is effective, light, robust, compact and cheap. We use a minimal number of sensors to reduce the size of the structure and simplify the algorithm. Specifically, three sensors are mounted on the robot hand for localizing a nearby object and providing error signals that drive the hand in three dimensions based on a potential energy algorithm. The minimum potential energy corresponds to the pre-grasp position that the hand converges to. At the same time, teleoperation also affects the trajectory of the hand; therefore, the combined result enables the end-effector to follow teleoperation and also track the object. To evaluate the performance of the system, experiments were conducted, including grasping a large number of regular and irregular objects, tuning the ratio of teleoperation to assistance and tracking a slow-moving object. The experiments were performed using 7-degree-of-freedom (DOF) MEKA arm and 5-DOF compliant MEKA hand.

The main features of the proposed system include the following:

1. An intuitive human–robot interface that combines the advantages of having human initiative, and the accuracy and robustness of a robotic system.
2. Little object knowledge is needed. The proposed IR strategy is to grasp objects with limited perception data. The three IR sensors used in the current approach only provide one-dimension data, but control the robot hand in 3 DOFs of translation and 2 DOFs of rotation.
3. Online adjustment of the robot hand to a suitable pre-grasp position relative to unknown objects without requiring premature object contact or regrasping strategies.
4. The system is robust when grasping a wide range of objects and tracking slow-moving objects.
5. The system employs low cost IR proximity sensors, which can be mounted on the robot hand easily without changing the structure of the hand.

2. Grasp Assistance

This section details how teleoperation grasp assistance is achieved by an array of three IR sensors mounted on the hand. We provide an overview of the process as follows. Firstly, the robot hand

https://doi.org/10.1017/S0263574714000733 Published online by Cambridge University Press

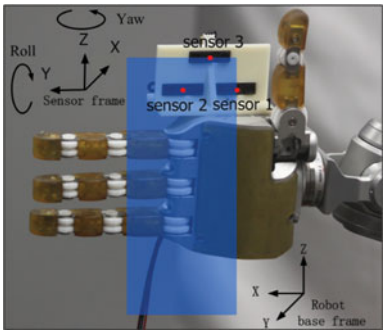


Fig. 1. IR sensor array: The red points are the centres of the sensors, and the blue rectangle is the projection of the object whose edges are to be aligned with the centres of sensors 1 and 3.

autonomously moves to a suitable pre-grasp position if at least one of the three sensors detects an object. Secondly, the robot hand avoids collision by keeping a distance to any object. With more sensors detecting the object, the distance would be larger. Thirdly, the end-effector is able to track a slow-moving object. Lastly, hand orientation is adjusted according to the object surface, so that it can avoid collision of the robot fingers with polygon objects.

Teleoperation of the robot hand is based on our previous work.[23] KINECT is employed as the sensor to collect Cartesian position data of the human arm joints, which the robot maps to its own internal coordinates so as to mimic human trajectories. At the same time, recognition of the human hand gesture as open or closed provides the signal for the robot to open or close its hand.

2.1. Infrared sensor array

Infrared proximity sensors (short range—Sharp GP2D120XJ00F) are employed in this paper. After calibration, the range of each IR sensor is [4 cm, 12 cm]. These IR sensors are efficient, robust and less sensitive to light, which satisfy our requirements of online grasp adjustments from a pre-grasp point. In addition, IR sensors involve much lower computational complexity compared with 3D sensors. This is crucial for real-time feedback in our system.

In order to improve the stability of grasping, the object should be wrapped in the curve of the palm and have enough contact area with the palm in the z-direction so that the array of sensors is mounted above the palm. These are arranged in a triangle layout as shown in Fig. 1 for adjusting the robot hand in the x, y and z-directions. All three sensors lie on a plane facing the x-direction. Sensors 1 and 3 are arranged in this configuration to find, respectively, the y- and z-direction edges of the object with respect to the sensor frame. If the sensors are too close to each other, sensor 2 may overshoot the object edge along with sensors 1 and 3, leading to the loss of all object signals. On the other hand, if the distances among sensors are too large, the size of the structure would be large and unsuitable for small objects. Thus, we design the distance between the sensors as 4–5 cm. Based on the sensor configuration, we assume that the objects to be grasped are not too small. The minimum size of the object is $y_{\min} \times z_{\min}$ on the y–z plane, where $y_{\min}$ is the distance between sensors 1 and 2 in the y direction, and $z_{\min}$ is the distance from sensor 3 to the palm in the z-direction.

2.2. Adjustment for positioning

Given a series of observations from the sensors, the goal is to search for the edges of the object.

We assume that the object is isolated. When the hand is close to the object, the signals from the IR sensors are used to construct a potential field, U_{IR}. The hand then moves to a desired pre-grasp location corresponding to the minimum of the sum of the following potential functions:

$$U_{\mathrm{IR}x} = \frac{1}{2}[(r_1 - a_1)^2 + (r_2 - a_2)^2 + (r_3 - a_3)^2], \tag{1}$$

$$U_{\mathrm{IR}y} = \frac{1}{2}(r_1 - a_1)^2, \tag{2}$$

$$U_{\mathrm{IR}z} = \frac{1}{2}(r_3 - a_3)^2, \tag{3}$$

https://doi.org/10.1017/S0263574714000733 Published online by Cambridge University Press

where a_i is the desired r_i value for the ith sensor corresponding to the pre-grasp position, and $r_i \in [l_{\min}, l_{\max}]$ is the detected distance of the object from the ith sensor, with $l_{\min}$ and $l_{\max}$ being the minimum and maximum sensing range respectively. In particular, $l_{\min}$ is the distance from the sensor plane to the palm surface in the x-direction, and $l_{\max}$ is the graspable distance from the hand to the object.

If all three sensors cannot detect any object, U_{IR} is zero. Therefore, the execution of the assisted pre-grasp motion depends on the initial placement. On the contrary, if any one of the sensors detects an object, then U_{IR} has values.

In the y-direction (see Eq. (4)), let the sensor reading be $r_1 = r_c$ on the surface close to the edge. On the edge, r_1 is in the range $[r_c, l_{\max}]$, so $a_1 \in [r_c, l_{\max}]$ represents the edge. Consequently, object edge detection involves searching for the point that satisfies $r_1 = a_1$. Based on empirical trials, we found that a_1 should be close to but less than $l_{\max}$. This enables the hand to move in the positive y-direction slowly to avoid vibrations caused by changing direction too frequently when sensor 1 is near the edge of the object. If sensor 1 detects the object ($r_1 < a_1$), the hand moves in the negative y-direction. If the sensor does not detect the object ($r_1 > a_1$), the hand moves in the positive y-direction. Thus, we have

$$\begin{cases} r_1 < a_1, & \textit{move in the negative y-direction} \\ r_1 = a_1, & \textit{stable in the y-direction} \\ r_1 > a_1, & \textit{move in the positive y-direction} \end{cases}. \tag{4}$$

The motion in the z-direction is determined by a similar rule:

$$\begin{cases} r_3 < a_3, & \textit{move in the positive z-direction} \\ r_3 = a_3, & \textit{stable in the z-direction} \\ r_3 > a_3, & \textit{move in the negative z-direction} \end{cases}. \tag{5}$$

In the x-direction (see Eq. (7)), the motion is described as follows. If more than one sensor detects the object, $r_1 + r_2 + r_3$ may become small, and the hand may move in the y- or z-direction. In this case, the hand keeps a distance from the object to avoid hitting the object.

If sensors 1 and 3 cannot detect the object, while sensor 2 can, r_1 and r_3 are equal to $l_{\max}$, and r_2 becomes smaller as U_x is minimized. Thus, the hand moves towards the object and keeps a shorter distance from the object compared with the previous case.

The values of a_i should satisfy the following condition:

$$a_1 + a_2 + a_3 = d + 2l_{\max}, \tag{6}$$

where d is the ideal distance from the sensor to the object for grasping. Therefore, when sensors 1 and 3 do not detect the object ($r_1 = r_3 = l_{\max}$), r_2 converges to d, which enables the robot hand to close and grasp the object. Hence, a_2 can be calculated from (6). Thus, we have

$$\begin{cases} r_1 + r_2 + r_3 < a_1 + a_2 + a_3, & \textit{move in the positive x-direction} \\ r_1 + r_2 + r_3 = a_1 + a_2 + a_3, & \textit{stable in the x-direction} \\ r_1 + r_2 + r_3 > a_1 + a_2 + a_3, & \textit{move in the negative x-direction} \end{cases}. \tag{7}$$

From (1), it is clear that all sensors contribute equally to the motion in the x-direction. Thus, in some particular cases, such as grasping slim objects, the hand may move close to the object, no matter which sensor detects the object while the other two sensor readings are $l_{\max}$. This enables the robot to robustly grasp a wide range of objects.

https://doi.org/10.1017/S0263574714000733 Published online by Cambridge University Press

Next, we design virtual forces that drive the desired hand position. The virtual forces are derived from potential energy as follows:

$$F_x = -\nabla U_{\mathrm{IR}x} = -[(r_1 - a_1) + (r_2 - a_2) + (r_3 - a_3)], \tag{8}$$

$$F_y = -\nabla U_{\mathrm{IR}y} = -(r_1 - a_1), \tag{9}$$

$$F_z = -\nabla U_{\mathrm{IR}z} = -(r_3 - a_3), \tag{10}$$

where ∇U_{IR} is the change in the potential energy associated with that particular force. It is derived by:

$$\nabla U_{\mathrm{IR}} = \frac{\partial U_{\mathrm{IR}}}{\partial r_1} + \frac{\partial U_{\mathrm{IR}}}{\partial r_2} + \frac{\partial U_{\mathrm{IR}}}{\partial r_3}. \tag{11}$$

This virtual force vector is fed to a virtual mass-damper system to derive the desired hand position:

$$F = m\ddot{x} + k\dot{x}, \tag{12}$$

where $m\ddot{x}$ is the component of inertial force and $k\dot{x}$ is the component of damping force. Then the desired hand positions ξ_{IR_x}, ξ_{IR_y} and ξ_{IR_z} are generated by

$$\ddot{\xi}_{\mathrm{IR}_x} = -c_x\dot{\xi}_{\mathrm{IR}_x} + F_x, \tag{13}$$

$$\ddot{\xi}_{\mathrm{IR}_y} = -c_y\dot{\xi}_{\mathrm{IR}_y} - F_y, \tag{14}$$

$$\ddot{\xi}_{\mathrm{IR}_z} = -c_z\dot{\xi}_{\mathrm{IR}_z} + F_z, \tag{15}$$

where $c_x > 0$, $c_y > 0$ and $c_z > 0$ are the parameters to tune the damping. Since a positive force drives the hand in the negative direction, the coefficient of F_y is negative in (14), unlike those of F_x and F_z (see Eqs. (13) and (15)).

2.3. Adjustment for orientation

To grasp a polygon robustly, we develop an additional algorithm based on potential energy for adjusting the robot hand orientation. Thus, the robot can tune the orientation of the hand autonomously using this algorithm before performing the adjustment of positions. It is assumed that all three sensors detect the same flat surface. To simplify the algorithm, only roll and yaw of the hand are considered. We define:

$$U_{\mathrm{IR}\alpha} = \frac{1}{2}\left[(r_3 - r_2)^2\right], \tag{16}$$

$$U_{\mathrm{IR}\gamma} = \frac{1}{2}\left[(r_1 - r_2)^2\right], \tag{17}$$

where the subscripts α and γ denote the roll and yaw orientations of the hand respectively.

The adjustment strategy for the roll orientation is that if the value of sensor 3 is less than that of sensor 2, the hand should rotate in the negative roll direction to decrease difference in the values between sensors 3 and 2. If $r_3 > r_2$, then the hand should rotate in the opposite direction. This is summarized as follows:

$$\begin{cases} r_3 < r_2, & \textit{rotate in negative roll direction} \\ r_3 = r_2, & \textit{stable in roll orientation} \\ r_3 > r_2, & \textit{rotate in positive roll direction} \end{cases}. \tag{18}$$

The adjustment strategy for the yaw orientation is similar to that of the roll orientation, but involves

https://doi.org/10.1017/S0263574714000733 Published online by Cambridge University Press

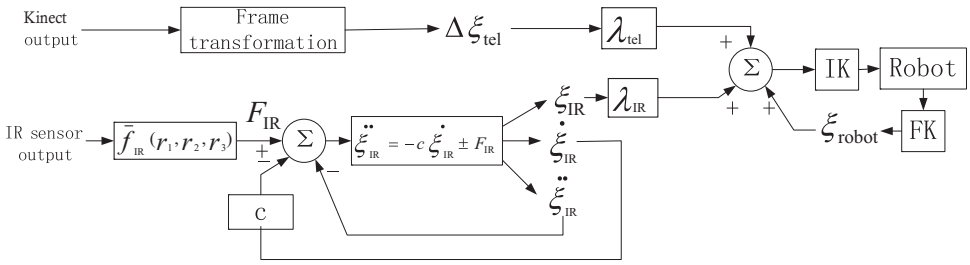


Fig. 2. Control block diagram. FK and IK denote forward and inverse kinematics maps respectively. $\overline{f}_{IR}$ is [8, 9, 10].

sensors 1 and 2 instead. It is summarized as follows:

$$\begin{cases} r_1 < r_2, & \textit{rotate in positive yaw direction} \\ r_1 = r_2, & \textit{stable in yaw orientation} \\ r_1 > r_2, & \textit{rotate in negative yaw direction} \end{cases}. \tag{19}$$

To realize the above-mentioned orientation adjustment strategies, the following virtual forces are generated:

$$F_\alpha = -\nabla U_{IR\alpha} = -(r_3 - r_2), \tag{20}$$

$$F_\gamma = -\nabla U_{IR\gamma} = -(r_1 - r_2). \tag{21}$$

The desired angles of roll and yaw orientations can be computed using:

$$\ddot{\alpha} = -c_\alpha \dot{\alpha} + F_\alpha, \tag{22}$$

$$\ddot{\gamma} = -c_\gamma \dot{\gamma} - F_\gamma, \tag{23}$$

where $c_\alpha > 0$ and $c_\gamma > 0$ and $c_z > 0$ are the parameters to tune damping.

2.4. Assistive teleoperated grasping

In this section, we integrate the position adjustment with human teleoperation to achieve assistive teleoperated grasping.

From the full teleoperation mode, if one or more sensors detect an object, the system will be converted to a combined system as illustrated in Fig. 2.

In the combined system, in order to match the data from the IR algorithm, the teleoperation output is chosen as the robot hand position with fixed orientation. The hand position is obtained by calculating forward kinematics. The positions at time points $t_1, t_2, t_3, ...$, are denoted by $\Delta\xi_{tel}(t_1)$, $\Delta\xi_{tel}(t_2)$, $\Delta\xi_{tel}(t_3)$, ..., where $\Delta\xi_{tel}(t_i)$ is the position changed during teleoperation. The final position is given by:

$$\xi(t_i) = \lambda_{IR}\xi_{IR} + \lambda_{tel}\Delta\xi_{tel}(t_i) + \xi(t_{i-1}), \tag{24}$$

where ξ_{IR} is the position from the IR algorithm, ξ is the position obtained from combining teleoperation and the IR algorithm, and $\lambda_{tel} > 0$ and $\lambda_{IR} > 0$ are the weighting parameters satisfying

$$\lambda_{IR} + \lambda_{tel} = 1. \tag{25}$$

3. Experimental Setup and Results

This section presents studies on evaluating the effectiveness of the proposed teleoperated grasping shared control, selecting the ratio of teleoperation to autonomy, tracking slow-moving objects,

https://doi.org/10.1017/S0263574714000733 Published online by Cambridge University Press



Fig. 3. 2D visual feedback from a display screen.

experimenting with graspable area and graspable objects and assessing the performance of the orientation adjustment algorithm.

3.1. Shared control

The ratio of teleoperation to autonomy

$$r = \frac{\lambda_{\text{tel}}}{\lambda_{\text{IR}}} \tag{26}$$

is an important factor affecting the ease of use of the system. We conducted an experiment that investigated the effect of this ratio and estimated an optimal value for shared control of teleoperated grasping.

Five healthy right-handed subjects, comprising three males and two females (subject 3 and subject 4), participated in this experiment. All subjects were naive to robot teleoperation, and two subjects were naive to robotics in general. The experimental task was to teleoperate the robot arm to grasp an object, namely a beverage can. The object position was fixed, and the initial positions of the robot and the subject were similar for every trial. Before data collection, each subject was given a session to familiarize himself/herself with the system, by performing 10 "full-teleoperation" and 10 "full-autonomy" trials. The "full-teleoperation" trials were such that both positioning and closing of the robot hand were teleoperated by human. The "full-autonomy" trials were such that positioning of the robot hand was initially teleoperated by human, but once the object was detected by IR sensors, autonomous positioning and grasping took over completely and the human no longer had any control. Also, each subject was instructed on how to use the IR-based control, in this the robot hand, on detection of the object, moved to grasp the object autonomously, but he/she could continue to move his/her hand to position the robot hand. When the sensors detected the object, audio feedback, in the form of a "beep," was sounded to the subject. When the output of sensor 2 is less than 5 cm, the robot hand and the object are close in the x-direction. At the same time, when the output of sensors 1 and 3 are larger than 10 cm, it is considered that the object edges are detected. When these conditions were met, the object was considered to be at a graspable position, and the robot hand closed automatically. The subject could also raise his/her left hand as a "manual override" command for closing the robot hand. Visual feedback was obtained from a monitor showing a video streamed from a monocular camera mounted on the robot head. Both object and robot hand could be seen clearly from this view (see Fig. 3). In the experiment, the value of the ratio r was varied from the set $\Omega_r = \{0, 0.5, 1, 2, \infty\}$, where $r = \infty$ refers to the full teleoperation mode with $\lambda_{\text{IR}} = 0$. Each subject performed a total of 50 trials over 10 sessions, i.e. each session contained five trials. The order of r chosen from Ω_r was randomized, and subjects were not aware of the r values.

IR sensors can improve the ability to grasp objects during teleoperation. Table I shows the success rates, which we denote by s_r, for different values of r. Without IR sensors, the uncertainty of teleoperation, which is the main cause of the low success rate for $r = +\infty$, cannot be ignored. It was difficult for the subject to localize the robot hand accurately due to the lack of depth information in the 2D visual feedback. In addition, different dimensions between human and robot arms posed difficulty for accurate grasping. On the contrary, with IR sensors, the user only needed to roughly drive the robot hand close to the object, and the robot would search for the object autonomously.

https://doi.org/10.1017/S0263574714000733 Published online by Cambridge University Press

Table I. Grasping success rates with different ratios of teleoperation and IR algorithm.

r	0	0.5	1	2	$+\infty$
Subject 1	9/10	10/10	10/10	9/10	7/10
Subject 2	8/10	10/10	10/10	7/10	3/10
Subject 3	8/10	9/10	9/10	9/10	2/10
Subject 4	7/10	9/10	9/10	9/10	3/10
Subject 5	8/10	8/10	8/10	9/10	6/10

Although human error could not be eliminated, the success rate with IR-based grasp assistance was significantly improved.

We quantify the effectiveness of teleoperation by two measures: effort in grasp placements, and error recovery ability. We define effort in grasping placement as

$$e = s \cdot t, \tag{27}$$

where t is the total duration starting from the time an object is detected to the time the hand arrives at the pre-grasp points, s is the distance of travel of the end-effector during t and e is the effort in grasping placement, which reflects the time and end-effector movement during positioning.

The samples in Fig. 4 are those of successful grasping from Table I. From the general trend of the five subjects, with larger r, the effort is larger. If the influence of the IR algorithm is too small, such as $r = +\infty$, the person has to manually teleoperate the end-effector to the desired position with great effort, since it is very hard to drive the end-effector to the intended position with teleoperation delay and only 2D visual feedback. In this case, the end-effector will likely travel over a longer distance and duration, i.e. greater effort.

On the other hand, the error recovery ability refers to the ease by which the robot hand trajectory can be altered to the intended one after the sensors detect a wrong object. In our experiment, we quantify it as the distance of the real position of end-effector with the proposed IR algorithm from the ideal position with full teleoperation. High error recovery ability allows ease of manual override when the robot tracks a wrong object. In our experiment, the user teleoperates the robot hand to move close to an object before moving away. The error of end-effector from the final position to the desired position of teleoperation, denoted by υ, can be seen in Fig. 5. It is obvious that with larger influence of teleoperation, the recovery ability is larger.

Figure 6 shows an example of the user driving the robot hand to approach and then move away from an object. For ease of comparison, teleoperation is simulated by the recorded data as seen in Fig. 6(f), and the rest (Figs. 6(a–e)) use this teleoperation data. Figures 6(a) to (e) illustrate different effects using different ratios from $r = 0$ to ∞. Generally, the system was entirely teleoperative until the sensors detected an object. With less teleoperation, it was able to track the object more accurately as shown in Figs. 6(a–c). However, more teleoperation enabled the users to change the trajectories more easily according to their will, as shown in Fig. 6(d–e).

In order to get an optimal parameter of r, all of the above conditions, including success rates, effort in grasping placement and error in final position, are considered. The criterion function that we seek to minimize to determine r is defined as

$$\phi_r = \begin{cases} \dfrac{\upsilon_r - \min(\upsilon)}{\max(\upsilon) - \min(\upsilon)}, & \textit{if error recovery trial} \\ \dfrac{1}{s_r} \cdot \dfrac{e_r - \min(e)}{\max(e) - \min(e)}, & \textit{if grasping trial} \end{cases}. \tag{28}$$

where s_r is the success rate in Table I.

https://doi.org/10.1017/S0263574714000733 Published online by Cambridge University Press

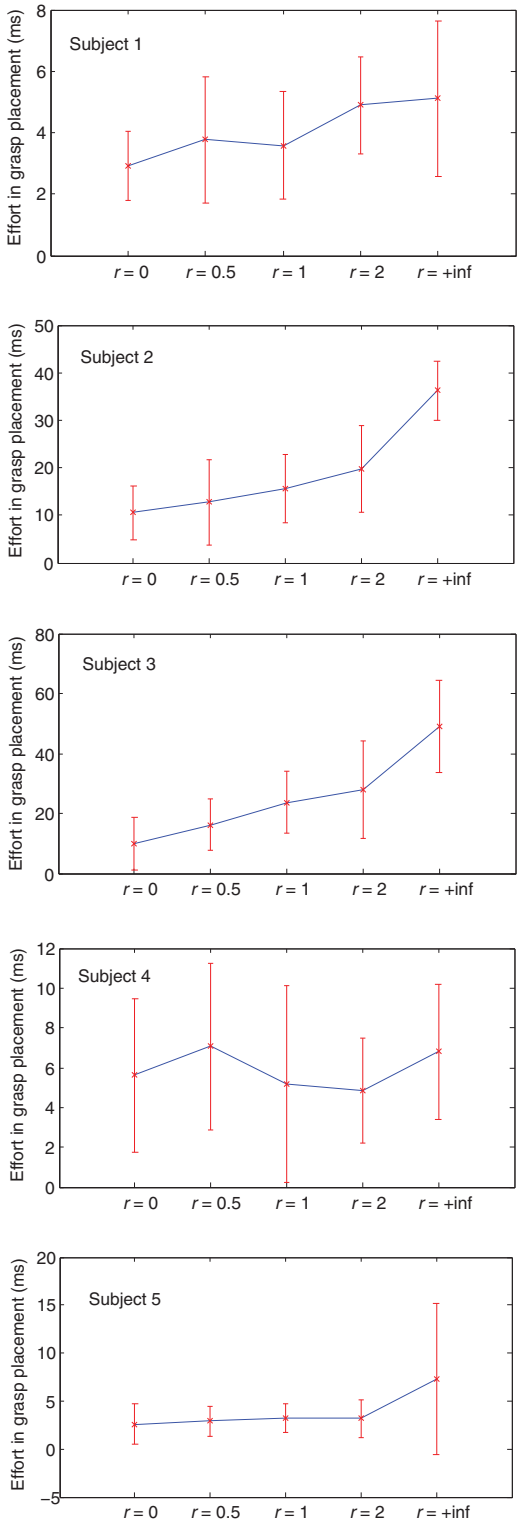


Fig. 4. Effort in grasp placement for different ratios of teleoperation to assistance. Mean values and standard deviations are shown.

Since e in (27) is based on the condition of successful grasps, the case of grasping trial should take into account the effect of the success rate s_r. A small ϕ suggests that effort in grasp placement or error in final position is less, and the success rate is higher. Hence, from Fig. 7, the optimal choice for r is around $r = 1$, which gives the least combined effort and final error with a small standard deviation.

https://doi.org/10.1017/S0263574714000733 Published online by Cambridge University Press

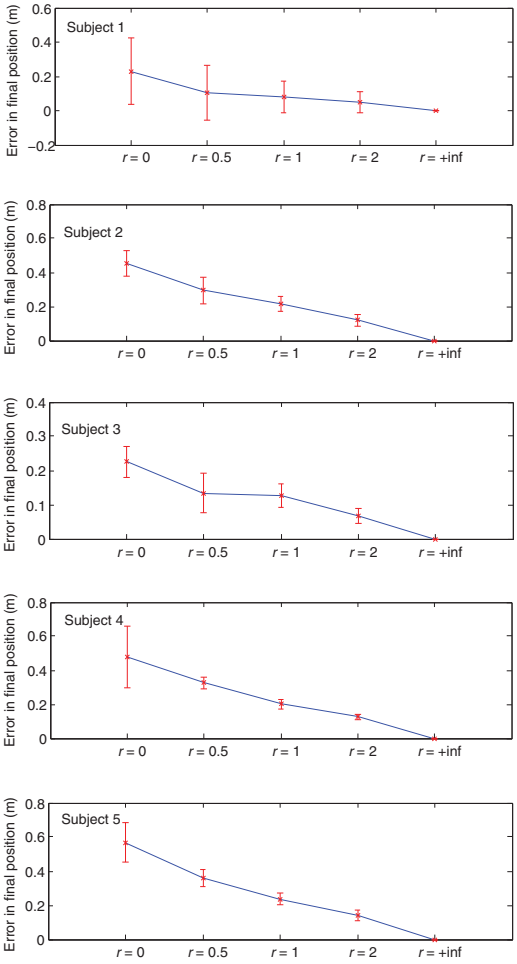
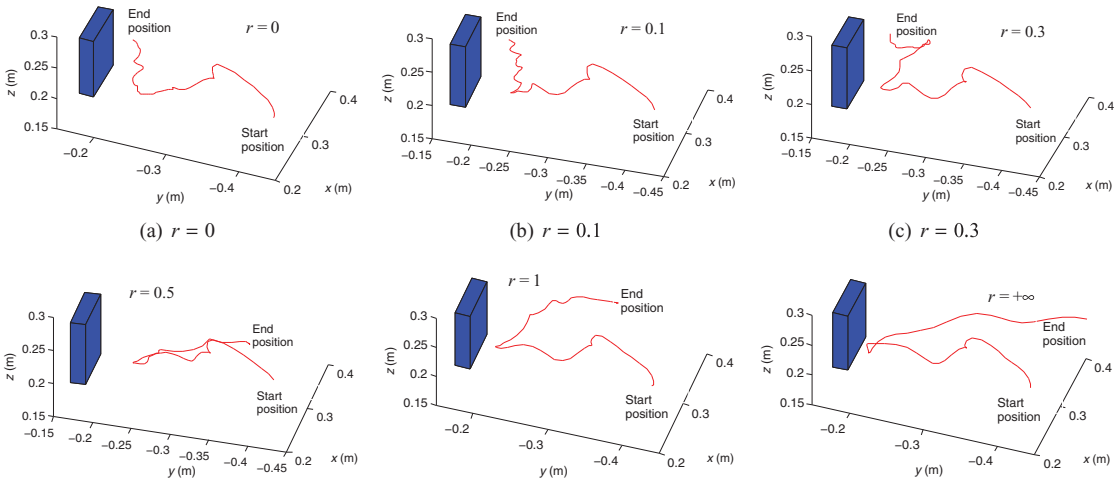


Fig. 5. Error in final position (υ) for different ratios of teleoperation to assistance. Mean values and standard deviations are shown.



(a) $r = 0$ (b) $r = 0.1$ (c) $r = 0.3$

(d) $r = 0.5$ (e) $r = 1$ (f) $r = +\infty$

Fig. 6. Robot hand trajectories relative to the rectangular object for different r values during error recovery trials.

https://doi.org/10.1017/S0263574714000733 Published online by Cambridge University Press

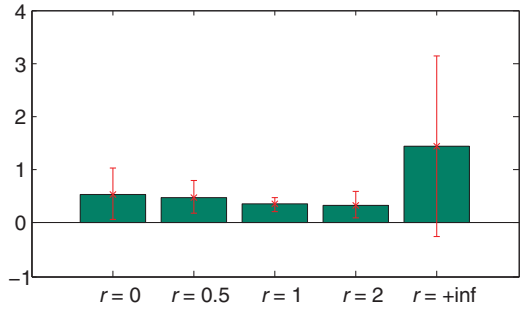


Fig. 7. Minimization criterion ϕ for different r values. Mean values and standard deviations are shown.

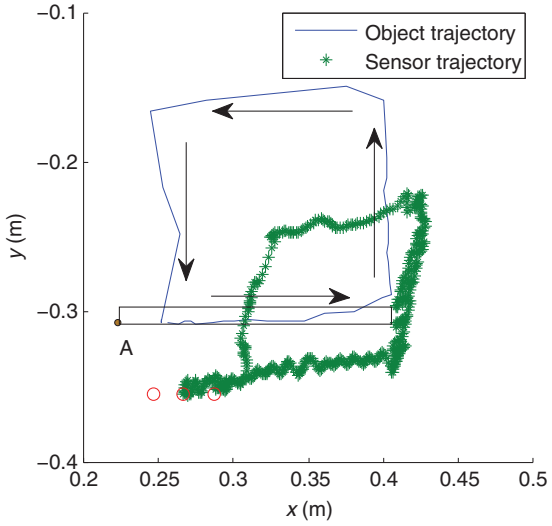


Fig. 8. Tracking a slow-moving object. The black rectangle is the object, and "A" is the lower left corner of the top xy face of the object. The blue line is the path taken by the object. The green asterisks show the path taken by sensor 3. The three red circles represent the initial position of the three sensors. The coordinates are with respect to the robot base frame.

It allows the robot hand to move away from the object if intended by the user, but generates a stable grasp automatically in the absence of user intervention.

3.2. Tracking slow-moving object

This proposed IR algorithm enables the robot to not only grasp a stationary object robustly but also track it while it is moving slowly. To test the tracking ability, a box whose position is marked by the lower left corner of the top xy face of the box, labeled "A" in Fig. 8, is slowly translated by hand so that the point "A" roughly traces a 15×15 cm^2. The orientation of the box remains constant throughout the movement. This experiment is only performed in the x–y plane, since the result in the z-direction is similar to that in the y-direction. Figure 8 shows the paths taken by sensor 3 and the object in the x–y plane after the tracking task, and Fig. 9 shows the trajectories in the x- and y-directions. In the top graph of Fig. 9, when the object is moving in the positive x-direction, only sensor 2 can detect the object; therefore, the distance of the object from the sensor array is small, and sensor 3 has almost the same trajectory with point A. When the object is moving in the positive y-direction, sensor 1 is pointing just off the left edge of the object face parallel to the x-direction, resulting in an offset between the object and sensor 3. After that, sensor 1 also detects the object, and the offset becomes larger. In the bottom graph of Fig. 9, when the object is moving in the positive y-direction, only sensor 2 can detect the object as stated above. However, both sensors 1 and 2 can

https://doi.org/10.1017/S0263574714000733 Published online by Cambridge University Press

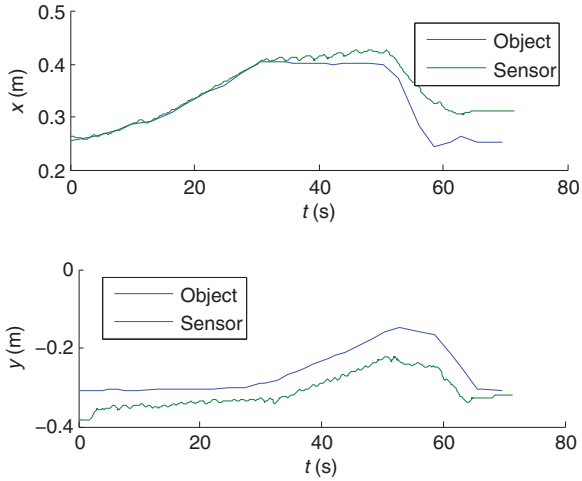


Fig. 9. Trajectories of sensor 3 and the object during the tracking task.

detect the object most of the time in the opposite direction, and the distance from the sensor to the object is large. This is the reason why the trajectory length is less than 15 cm in the y-direction.

3.3. Graspable areas

The graspable area for the IR algorithm is experimentally verified for sample objects, including objects with circular and rectangular cross sections. In the experiment, the sensor initial positions are fixed, and the objects are put on the vertices of a grid in different trials. If the sensors could detect the object and the hand could grasp the object successfully, the position of the object would be marked. This experiment only considers the x–y plane, and the grid points are of 1-cm intervals. In Fig. 10, the cross "$\times$" represents the center of the surface facing the IR sensors. If the distance from the object to sensor is more than 12 cm, the hand is unlikely to grasp the object. At the same time, the object cannot be too close to the hand so as to avoid collision. The range of sensors are [4 cm, 12 cm], and the distance of the sensor to the hollow of the palm is 3–4.5 cm; therefore, the available range in the x-direction should be around 8.5–9 cm for rectangular object. The width of the object (cube) surface facing the IR sensors is 6 cm, and the distance between sensors 1 and 2 is 4 cm; therefore, the available range in the y-direction should be around 10 cm for rectangular object. Hence, with some tolerance of sensor noises and errors, the graspable area is very close to expectation. It is similar for other shape objects such as circular objects (see Fig. 10(b)).

3.4. Graspable objects

The proposed method enables a robot to grasp a wide range of regular and irregular objects as long as the objects are not too small. For ease of analysis, the experiments in this section are based on an entirely autonomous mode of operation without teleoperation. In addition, it employs the algorithm of positioning adjustment but not orientation adjustment.

As can be seen in Fig. 11, a person hands over an object to the robot in the range of IR sensors, but out of range of a direct grasp. Then the robot hand moves to a pre-grasp position and closes the hand to grasp the objects. Irregular objects, such as a cutter, tape, and toy hand as well as slim objects, such as a marker pen, can be stably grasped. If only one sensor detects the object, the hand will also move close to the object, thus ensuring that slim objects can also be grasped. In addition, the sensors are close enough to each other so that even slim objects are detected by at least one sensor.

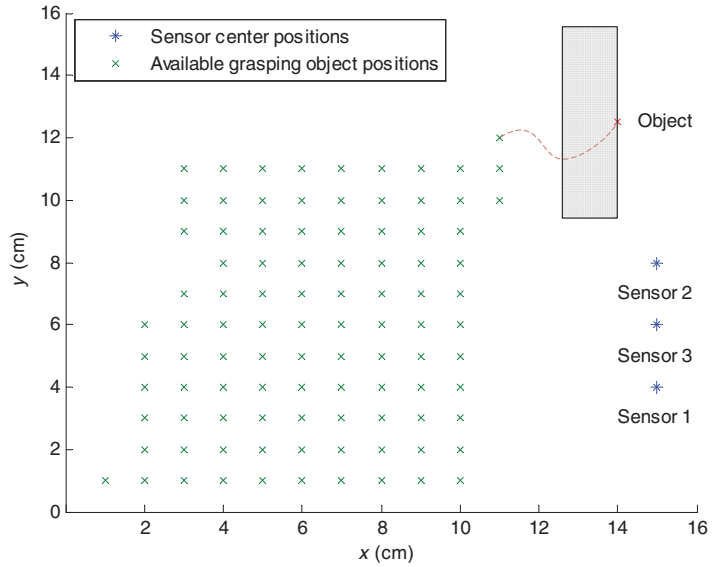
However, it fails to grasp transparent objects, which is a limitation of IR sensors (see Fig. Fig 12(a)).

Unsuitable orientation is another reason of failure. To test the influence of orientation for positioning algorithm without orientation adjustment, a box is used as a goal object on the table

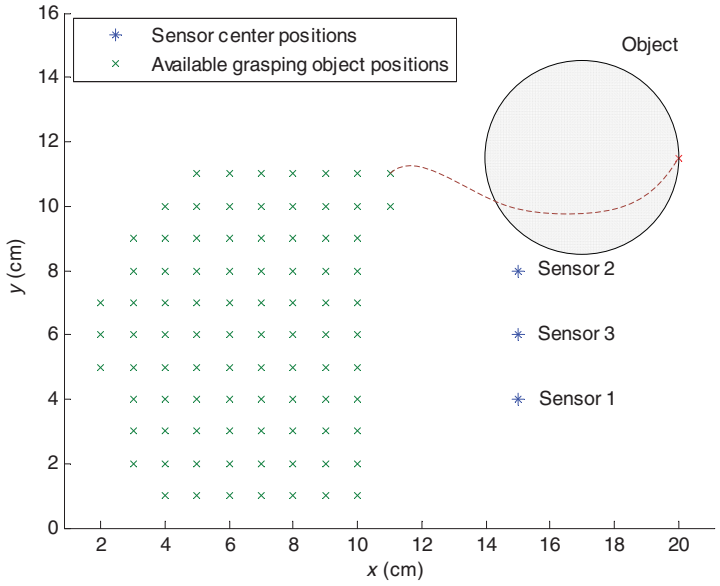
https://doi.org/10.1017/S0263574714000733 Published online by Cambridge University Press

Table II. Grasping success rates.

Degree	0	15	30	45	60	75	90	105	120	135	150	165
Success rate	5/5	5/5	5/5	5/5	5/5	5/5	5/5	3/5	2/5	0/5	5/5	5/5



(a) Graspable area map of a sample object with rectangular cross-section.



(b) Graspable area map of a sample object with circular cross-section.

Fig. 10. Graspable area maps verified experimentally. The shaded rectangle and circle are sample objects. End "×" represents the position of the center of the surface of the object facing IR sensors.

as shown in Fig. 13. The surface of the box towards the sensors has dimensions of 137 × 57 mm. The angle θ ranges from 0° to 180° in steps of 15°. The hand orientation is fixed, but the position varies according to the grasp algorithm. With $\theta \in [105, 135]^\circ$ (see Table II), the fingers may collide with the object as in Fig. 12(b).

https://doi.org/10.1017/S0263574714000733 Published online by Cambridge University Press

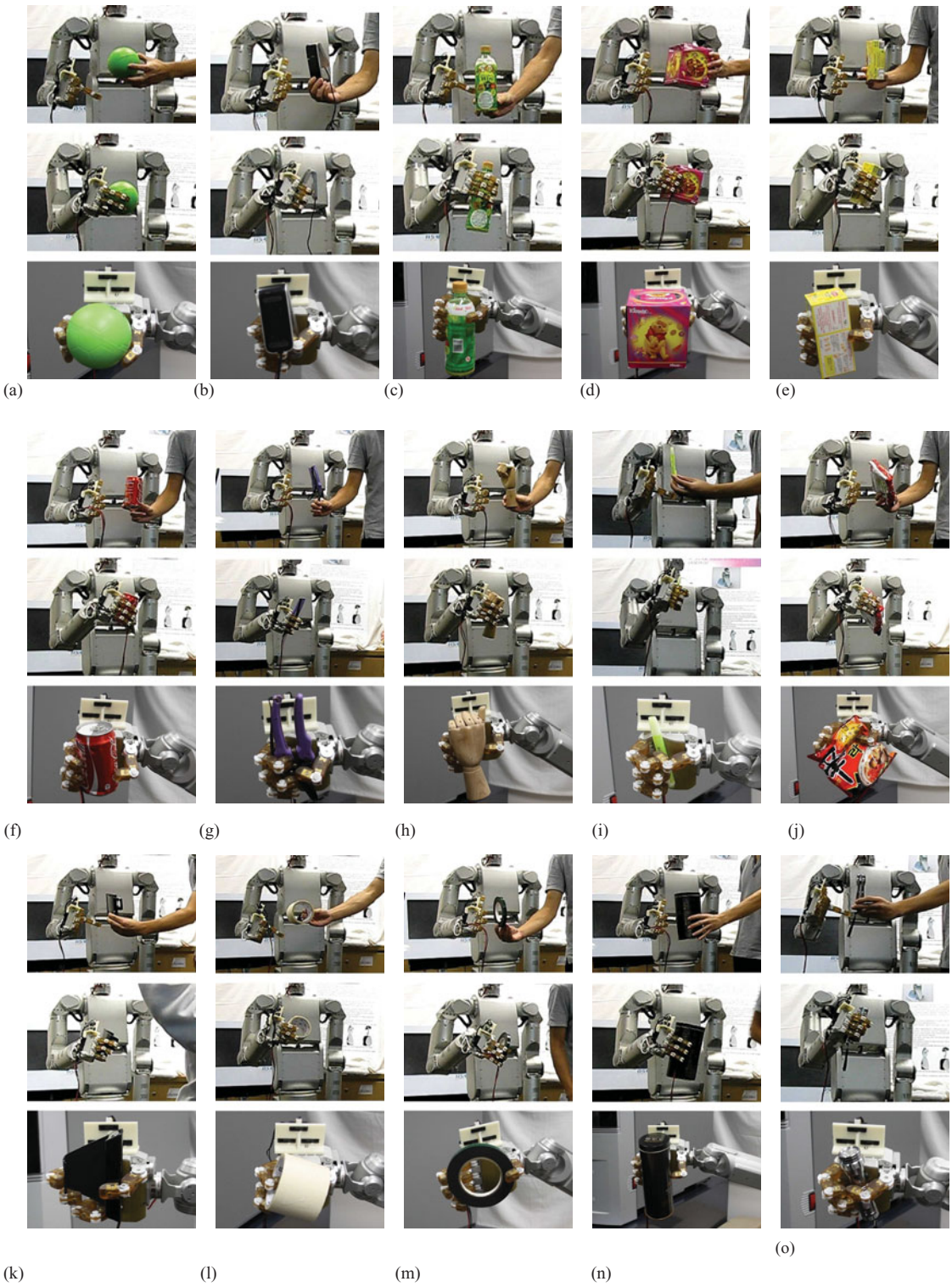
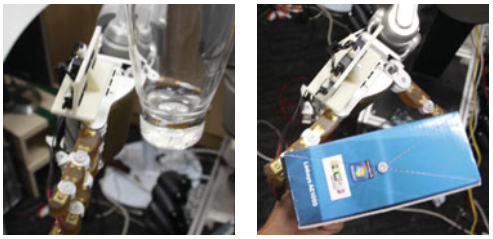


Fig. 11. Grasp experiments. For every object, the top picture shows the initial position of the sensor detecting an object. The middle and bottom pictures show the final grasp from front view and side view respectively.

https://doi.org/10.1017/S0263574714000733 Published online by Cambridge University Press



(a) Transparent object (b) Collision

Fig. 12. Failures of grasping.

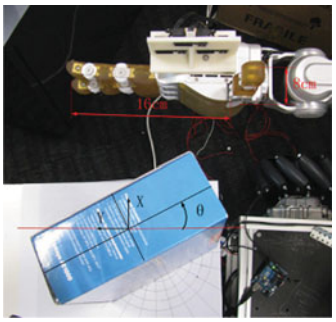


Fig. 13. Object rotation test.

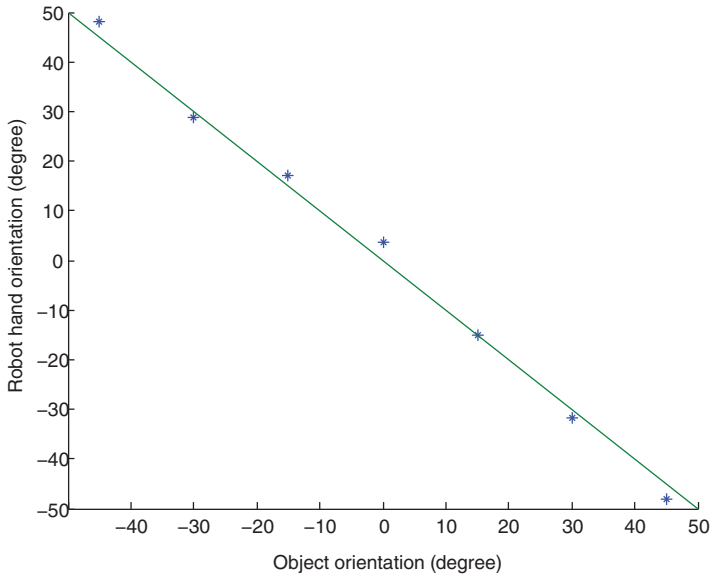


Fig. 14. Orientation result.

3.5. Adjustment of orientation

Unsuitable orientation may cause failure for grasping. While the orientation issue can be circumvented by teleoperation, it requires additional effort from the user. In this paper, we look into the orientation issue especially to achieve more autonomous grasping. The adjustment of orientation is developed to improve the system to become more intuitive.

In order to deal with the orientation issue, we explore the orientation adjustment algorithm. Figure 14 shows that the robot hand is able to fit the orientation of a cube. The experiment setup can be seen in Fig. 13, and the object is rotated about the z-axis by an angle θ that ranges from -45° to 45°. Only the results for the yaw orientation are shown; the results for the roll orientation are similar. The initial yaw orientation of the hand is 0° and the steady state yaw orientation after the algorithm

https://doi.org/10.1017/S0263574714000733 Published online by Cambridge University Press

converges is compared with the object orientation. In the seven samples, the maximum error between the hand orientation and the object orientation is 3.61°, while the minimum error is 0.16°. The result demonstrates that the robot hand is able to match the object orientation with the proposed algorithm.

4. Conclusions and Future Works

In this paper, we have presented an effective system that enables a robot to perform on-line adjustment of the final grasp during teleoperation. It is a novel method to deal with the challenge of uncertainty in the environment during teleoperated grasping. An array of three IR sensors is used for proximally sensing the object distance. This provides a corrective signal for the hand to close in on the object using a potential function-based algorithm. We have analysed user performance in a five-user study of teleoperated grasping, and selected optimal weighting parameters in the shared control scheme to improve the ease of teleoperated grasping. Comparing with full user teleoperation, our IR-based grasp assistance algorithm achieves greater grasping success rates and increases ease and efficiency of user control. In addition, experiment results demonstrate that a wide range of regular and irregular objects can be grasped, and slow-moving objects can be tracked robustly.

Acknowledgements

This work is supported by the A*STAR Science and Engineering Research Council (SERC) grant No. 1225100001.

References

1. L. Li, B. Cox, M. Diftler, S. Shelton and B. Rogers. "Development of a Telepresence Controlled Ambidextrous Robot for Space Applications," **In:** *Proceedings of the 1996 IEEE International Conference on Robotics and Automation*, vol. 1 (Apr. 1996) pp. 58–63.
2. D. Lee, O. Martinez-Palafox and M. Spong. "Bilateral Teleoperation of Multiple Cooperative Robots Over Delayed Communication Networks: Application," *Proceedings of the 2005 IEEE International Conference on Robotics and Automation (ICRA 2005)* (2005) pp. 366–371.
3. R. Ambrose, H. Aldridge, R. Askew, R. Burridge, W. Bluethmann, M. Diftler, C. Lovchik, D. Magruder and F. Rehnmark. "Robonaut: NASA's space humanoid," *IEEE Intell. Syst. Appl.* **15**(4), 57–63 (2000).
4. W. B. Griffin, W. R. Provancher and M. R. Cutkosky. "Feedback Strategies for Shared Control in Dexterous Telemanipulation," **In:** *Proceedings of the 2003 IEEE/RSJ International Conference on Intelligent Robots and Systems (IROS 2003)* , vol. 3 (Oct. 2003) pp. 2791–2796.
5. M. Fischer, P. van der Smagt and G. Hirzinger. "Learning Techniques in a Dataglove-Based Telemanipulation System for the DLR Hand," **In:** *Proceedings of the 1998 IEEE International Conference on Robotics and Automation*, vol. 2 (May 1998) pp. 1603–1608.
6. V. Popescu, G. Burdea, M. Bouzit and V. Hentz. "A virtual-reality-based telerehabilitation system with force feedback," *IEEE Trans. Inf. Technol. Biomed.* **4**(1), 45–51 (2000).
7. C. Lei, C. Ggo and J. S. Dai. "Kinematic Mapping and Calibration of the Thumb Motions for Teleoperating a Humanoid Robot Hand," *ASME 2011 International Design Engineering Technical Conferences and Computers and Information in Engineering Conference* (2011) pp. 1139–1147.
8. M. Popović, D. Kraft, L. Bodenhagen, E. Başeski, N. Pugeault, D. Kragic, T. Asfour and N. Krüger, "A strategy for grasping unknown objects based on co-planarity and colour information," *Robot. Auton. Syst.* **58**, 551–565 (2010).
9. A. Saxena, L. L. S. Wong and A. Y. Ng. "Learning grasp strategies with partial shape information," *AAAI* **3**(2), 1491–1494 (2008).
10. B. Wang, L. Jiang, J. LI and H. Cai. "Grasping Unknown Objects Based on 3D Model Reconstruction," *Proceedings of the 2005 IEEE/ASME International Conference on Advanced Intelligent Mechatronics* (2005) pp. 461–466.
11. C. C. Kemp, C. D. Anderson, A. J. Trevor and Z. Xu. "A Point-and-Click Interface for the Real World: Laser Designation of Objects for Mobile Manipulation," *Proceedings of the 3rd ACM/IEEE International Conference* (2008) pp. 241–248.
12. A. Jain and C. C. Kemp, "El-e: An assistive mobile manipulator that autonomously fetches objects from flat surfaces," *Auton. Robots* **28**(1), 45–64 (2009).
13. A. Petrovskaya, O. Khatib, S. Thrun and A. Ng, "Bayesian Estimation for Autonomous Object Manipulation Based on Tactile Sensors," *Proceedings of the 2006 IEEE International Conference on Robotics and Automation (ICRA)* (2006) pp. 707–714.
14. K. Hsiao, S. Chitta, M. Ciocarlie and E. Jones, "Contact-Reactive Grasping of Objects with Partial Shape Information," *2010 IEEE/RSJ International Conference on Intelligent Robots and Systems (IROS)* (2010) pp. 1228–1235.

https://doi.org/10.1017/S0263574714000733 Published online by Cambridge University Press

15. A. Leeper, K. Hsiao, E. Chu and J. K. Salisbury, "Using Near-Field Stereo Vision for Robotic Grasping in Cluttered Environments," **In:** *Experimental Robotics* (Springer Tracts in Advanced Robotics), (O. Khatib, V. Kumar and G. Sukhatme, eds.), vol. 79 (Springer Berlin Heidelberg, 2014) pp. 253–267.
16. J. Smith, E. Garcia, R. Wistort and G. Krishnamoorthy. "Electric Field Imaging Pretouch for Robotic Graspers," *IEEE/RSJ International Conference on Intelligent Robots and Systems (IROS'07)* (2007) pp. 676–683.
17. R. Wistort and J. Smith. "Electric Field Servoing for Robotic Manipulation," *IEEE/RSJ International Conference on Intelligent Robots and Systems (IROS'08)* (2008) pp. 494–499.
18. L.-T. Jiang and J. Smith. "Seashell Effect Pretouch Sensing for Robotic Grasping," *2012 IEEE International Conference on Robotics and Automation (ICRA)* (2012) pp. 2851–2858.
19. K. Hsiao, P. Nangeroni, M. Huber, A. Saxena and A. Y. Ng. "Reactive Grasping Using Optical Proximity Sensors," *IEEE International Conference on Robotics and Automation (ICRA'09)* (2009) pp. 2098–2105.
20. H. Kim, J. Biggs, W. Schloerb, M. Carmena, M. Lebedev, M. Nicolelis and M. Srinivasan, "Continuous shared control for stabilizing reaching and grasping with brain-machine interfaces," *IEEE Trans. Biomed. Eng.* **53**(6), 1164–1173 (2006).
21. M. Teichmann and B. Mishra. "Reactive robotics I: Reactive grasping with a modified gripper and multifingered hands," *Int. J. Robot. Res.* **19**(7), 697–708 (2000).
22. E. Rimon and D. Koditschek. "Exact robot navigation using artificial potential functions," *IEEE Trans. Robot. Autom.* **8**(5), 501–518 (1992).
23. N. Chen, C.-M. Chew, K. P. Tee and B. S. Han. "Human-Aided Robotic Grasping," *21st IEEE International Symposium on Robot and Human Interactive Communication (RO-MAN, 2012)* Paris, France (Sep. 9–13, 2012) pp. 75–80.

https://doi.org/10.1017/S0263574714000733 Published online by Cambridge University Press